POLITECNICO DI TORINO
Repository ISTITUZIONALE

Modeling of dark current in midinfrared quantum well infrared photodetectors

Original
Modeling of dark current in midinfrared quantum well infrared photodetectors / Castellano, F.; Rossi, Fausto; Faist, J.; Lhuillier, E.; Berger, V.. - In: PHYSICAL REVIEW. B, CONDENSED MATTER AND MATERIALS PHYSICS. - ISSN 1098-0121. - STAMPA. - 79:20(2009), pp. 205304-1-205304-10. [10.1103/PhysRevB.79.205304]

Availability:
This version is available at: 11583/2372314 since:

Publisher:
APS American Physical Society

Published
DOI:10.1103/PhysRevB.79.205304

Terms of use:
openAccess

This article is made available under terms and conditions as specified in the corresponding bibliographic description in the repository

Publisher copyright

(Article begins on next page)

27 November 2022

Modeling of dark current in midinfrared quantum well infrared photodetectors

Fabrizio Castellano and Fausto Rossi
Dipartimento di Fisica, Politecnico di Torino, Corso Duca degli Abruzzi 24, 10129 Torino, Italy

Jerome Faist
Quantum Optoelectronics Group, ETH Zurich, Wolfgang-Pauli-Strasse, Zurich, Switzerland

Emmanuel Lhuillier
Laboratoire MPQ, Université Paris Diderot–Paris 7, Bat Condorcet, Case 7021, 75205 Paris Cedex 13, France and Chemin de la Huniére, ONERA-DOTA, 91761 Palaiseau Cedex, France

Vincent Berger
Laboratoire MPQ, Université Paris Diderot–Paris 7, Bat Condorcet, Case 7021, 75205 Paris Cedex 13, France
(Received 27 January 2009; revised manuscript received 6 April 2009; published 6 May 2009)

We present a model for the description of dark *IV* curves in midinfrared quantum well infrared photodetectors at low temperatures, in a regime where dark current is dominated by interwell tunneling. The model separates the *IV* curve into a low-field and a high-field region allowing us to identify the effects ascribed to miniband transport and carrier localization, respectively. At low fields the system is thought as a superlattice and described by means of a high-density correction of the Esaki-Tsu model. This approach allows us to simulate current saturation phenomena that occur at low temperatures at intermediate fields. On the other hand, high-field transport effects are described in the localized Wannier-Stark basis in order to account for tunneling and field-assisted thermionic emission effects. We then compare simulations with our measurements of the *IV* curves of mid-IR quantum well infrared photodetectors finding good quantitative agreement between theory and experiment.

DOI: 10.1103/PhysRevB.79.205304 PACS number(s): 85.35.Be, 85.60.Bt, 73.63.−b

I. INTRODUCTION

Quantum well infrared photodetector (QWIP) technology has developed at a sustained pace in last years and now state of the art QWIPs in the midinfrared (MIR) spectral range are mature and reliable devices.[1] Whereas the main applications of QWIPs are dedicated to imagery in the atmospheric transparency windows (3–5 μm and 8–12 μm), new aerospace and defense applications have developed the interest for the 12–20 μm wavelength.

The presence of dark current in QWIPs is one of the main performance-limiting factors and as such has been the subject of intense research in the past.[2–6] It is now clear that for devices operating in the liquid nitrogen temperature range the dark current is caused by thermally excited carriers and thus shows an exponential dependence on temperature. The most common way of reducing the dark current in present-day QWIP-based infrared imagery systems is thus to reduce the operating temperature in the liquid nitrogen range until the desired performance requirements are met. Anyway the cost of the cryogenic coolers has a huge impact on system design and this is the reason why the operating temperature of common QWIP systems is not usually pushed too low.

In some aerospace and defense applications such constrain is relaxed and this allows to reduce the temperature down to a regime where dark current is dominated by tunneling rather than thermionic emission. Nevertheless because such applications usually involve very low photons fluxes, the reduction in dark current remains a crucial issue that cannot be addressed by further temperature reduction since the tunneling currents are independent of it.

Since the first step in technological optimization is the understanding of underlying physical processes, in the present paper we investigate the nature of dark current in QWIPs in the low-temperature regime by developing a simple model and ready interpretable model which is then used to justify the data measured from QWIPs that we have designed and grown.

The paper is organized as follows. In Sec. II we describe the device under study and present the *IV* measurements and then Sec. III contains a general description of the model we have developed. Finally in Sec. IV we apply the model to compute the *IV* curve of the device described in Sec. II and discuss our results.

II. EXPERIMENT

The device under study is a mid-IR QWIP composed of 40 $GaAs/Ga_{0.85}Al_{0.15}As$ periods, with 7.3 nm wells and 35 nm barriers (as shown in Fig. 2). The wells are *n* doped and the sheet density is $N_{2D}=3\times10^{11}$ cm^{-2}, corresponding to an average volume density $N_{3D}=2.13\times10^{-17}$ cm^{-3} over the supercell. This gives a Fermi energy of the electron population of 10.5 meV above the ground state.

IV measurements of QWIP have been made using a 6430 Keithley femtoamperemeter, whereas the component is placed on the cold finger of a circulation Janis cryostat. Temperature regulation is ensured by a 330 Lakeshore.

Figure 1 shows the current-voltage (*I-V*) curves of the device measured at temperatures ranging from 10 to 60 K showing qualitatively different behaviors as temperature in-

 ©2009 The American Physical Society

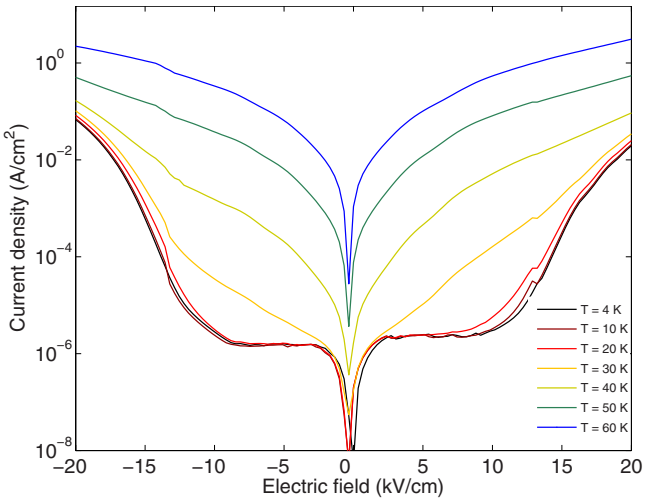

FIG. 1. (Color online) Current voltage characteristics of the device at different temperatures. The current shows no dependence on temperature up to 20 K, and then its roughly exponential increase denotes the onset of the thermionic regime.

creases. In particular, at low temperatures ($T<30$ K) some interesting features are present: after an initial increase the current shows a saturation resulting in a wide plateau region where it remains constant over a large bias range at a value of around 3×10^{-6} A/cm^2. Then starting from around 10 kV/cm the current starts to rapidly increase again up to 0.1 A/cm^2. The low-temperature curves show no dependence on the temperature itself over the whole bias range. Starting from 30 K additional features begin to show up in the plateau region and finally at high temperature the *IV* curves show a qualitatively different behavior: the plateau is no more present and the *IV* curve is constantly increasing over the whole electric field range toward an exponential asymptote.

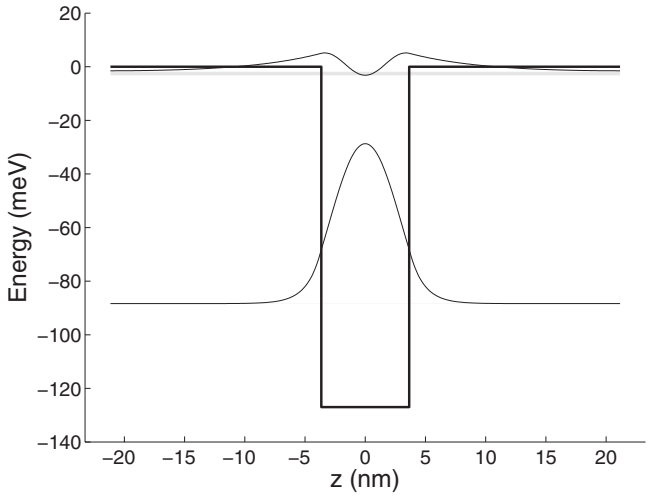

FIG. 2. Conduction band profile and normalized wave functions for the QWIP under study. The gray shaded regions represent the miniband along the growth direction.

III. MODELING

The complete *IV* curve family can be divided in three well separated regions where different transport mechanisms can be thought to apply. In the high-temperature regime the current is due to transport of thermally excited carriers in the continuum and well established models exist for its evaluation.[6] At low temperatures the continuum is not populated and the current can thus be only due to carriers moving across bound states, i.e., tunneling currents. The lack of temperature dependence of the tunneling current tells us that only electrons in the ground state are contributing to it. The shape of *IV* curves suggest the identification of two additional regimes, namely, a low-bias and a high-bias regime, each one characterized by a clear fingerprint: a saturating low-field current followed by a rapid increase at high biases. The aim of this paper is the clarification of the physics underlying these two regimes.

Since the barriers in QWIPs are usually very thick (20–70 nm) and the number of unit cells is usually sufficiently high to allow us to neglect the effect of contacts, transport can be thought as due to electrons moving in a weakly coupled superlattice along the growth direction z under the effect of an electric field. Although a huge amount of theoretical and experimental work has been carried out in the past regarding transport in superlattices, very little attention has been devoted to the weakly coupled case.[7] This is mainly due to the fact that physically relevant effects such as resonant tunneling and interminiband Zener transitions are much stronger in superlattices with thin barriers, where the gaps between minibands become comparable to the miniband width.

From these studies it has become clear that two well separated pictures might be applied to the study of transport in these systems: the miniband picture and the localized Wannier-Stark picture. These two pictures are now recognized to be formally equivalent[8] and reflect the well-known gauge freedom in electrodynamics: while in the miniband picture the bias field is taken as the time derivative of a vector potential with linear time dependence (but space independent), in the Wannier-Stark case the field is thought as the gradient of a time independent scalar potential. As a result the carrier transport process is described in two alternative ways. In the miniband picture the electric field has the role of increasing the electron wave vector along the direction of the field at a rate proportional to its intensity. In the Wannier-Stark picture there is no wave vector along the growth direction and the effect of the field is to change the interwell tunneling probabilities by modifying the shape of the barriers. They are thus just two different points of view of the same problem and the description of physical processes can be in theory carried on in both pictures correctly.

Anyway when dealing with numerical computation the Wannier-Stark based codes usually suffer from convergence problems due to the wave function delocalization at low fields, while nontrivial energy-nonconserving processes due to the time dependence of the basis appear in the miniband picture at high fields which are difficult to handle. Thus depending on the magnitude of the electric field, modeling (especially numerical calculations) is more easily handled in one of the two pictures: while miniband transport is usually

best suited to low-field regimes, the Wannier-Stark picture is better behaved in the opposite limit.

Moreover the separation between "low" and "high" electric fields cannot always be told with precision. When dealing with transport in a superlattice with spatial periodicity L_z subject to a constant electric field F along the growth direction it is commonly accepted that the miniband picture is valid when the Stark shift eFL_z is less than the typical energy scale of the miniband structure, while the Wannier-Stark picture applies otherwise. Such characteristic energy scale is usually taken as the miniband width ϵ, but in a system with multiple minibands this is not a unique parameter and the gaps between minibands might be used instead. In other words this amounts to evaluating how strong the Zener effects are and whether or not they can be neglected in the miniband picture.

A. Modeling strategy

The miniband structure of the device under study is computed by means of a plane-wave expansion of the Schrödinger equation within the effective mass approximation as described in Ref. 9. The zero-field conduction-band profile is taken to be piecewise constant with a barrier height of 128 meV, infinitely periodic along the growth direction and perfectly homogeneous along the in-plane directions. Considering 7.3 nm wells and 35 nm barriers the system shows two bound levels at energies $E_0=38.5$ meV and $E_1=124$ meV from the quantum well (QW) bottom giving rise to two minibands of width $\epsilon_1=30$ neV and $\epsilon_2=1.4$ meV.

Such numbers, especially the incredibly low ground miniband width, clearly tell us that the systems falls in the category of weakly coupled superlattices and also pose some problems in the definition of high- and low-field regime. While it is clear that the Stark shift is greater than both the miniband widths for any experimentally reasonable bias, the separation between the two bound levels, which amounts to 87 meV, corresponds to a bias of about 20 kV/cm which corresponds to the highest electric field applied to the device in our measurements.

In this situation there is no clear indication regarding which of the two pictures should best describe the problem but rather it is more likely that a model based on a transition between the miniband and the Wannier-Stark pictures should be developed. We decide to write the total current density j as the sum of different contributions

$$j = \sum_{\nu} j_{\nu} + j_{\nu \to c}, \tag{1}$$

where j_ν represent current components due to electrons in miniband ν, or alternatively, electrons that tunnel from the νth level of a QW to the corresponding νth level in the neighboring one. As we shall see, theses terms are dominant at very low fields, and thus are likely to be described by the miniband picture. The terms $j_{\nu \to c}$ are current contributions due to electrons tunneling from state ν directly into the continuum, a process which is dominant at very high fields, and thus these terms will be handled in the Wannier-Stark picture.

B. Low-temperature and low-bias regime

When the superlattice is subject to a very low electric field, as already mentioned, the miniband picture should be best suited to describe the problem. In addition, at very low temperatures, the excited state is not populated so we are dealing with a single miniband transport problem. This fact is also confirmed by the lack of temperature dependence of the current up to 30 K over the whole electric field range, which means that thermal activation of the upper miniband can be neglected. The characteristic feature of the *IV* curves shown in Fig. 1 in the low-field/low-temperature regime is a saturating behavior which results in a large plateau where the current remains independent of the applied bias.

Such behavior reminds of the well-known negative differential resistance effect in superlattices, which was first described by Esaki and Tsu[10] by means of a semiclassical single miniband transport model in the low-density limit. Such model was subsequently generalized to cases in which the Fermi energy may lie over the upper miniband edge by Lebwohl and Tsu.[11] Anyway such extension was carried on at zero temperature, where the Fermi-Dirac distribution is taken to be a unit step function. Such approximation is valid at low temperatures if the miniband width ϵ is greater than k_BT because in that case we can assume that the miniband is either filled, empty, or half-filled. In the present case such approximation cannot be applied because $\epsilon \ll k_BT$ for any reasonable temperature, thus we shall perform the computation again by assuming that the distribution function is slowly varying across the miniband (details can be found in Appendix A).

Surprisingly enough, the final result is the same as reported in Ref. 11 for $T=0$ and we can find the same analytical expression for ground miniband current,

$$j_0 = N_{3D} \frac{F\tau}{\frac{\hbar^2}{e^2 L_z^2} + (F\tau)^2} \frac{\epsilon^2}{8E_F} f(E_0). \tag{2}$$

where E_F is the electron Fermi energy, L_z is the potential periodicity, F is the electric field, ϵ is the miniband width, and $f(E_0)$ is the value of the Fermi-Dirac distribution at the lower edge of the ground miniband, which is 1 in the low-temperature regime since the Fermi energy is well above the ground state. The momentum relaxation time τ describes the time rate at which electrons are scattered back toward the center of the Brillouin zone and in this model has to be regarded as a free parameter, even though we shall see that it will not influence the final result.

Figure 3 shows the computed *IV* curve for different values of τ and the experimental data at 10 K. It can be seen that within this model the plateau current corresponds to the maximum of the Esaki-Tsu *IV* curve, after which the negative differential resistance region begins. The value of the momentum relaxation time τ defines the position and width of the maximum, giving rise to a wide plateau for $\tau=20$ fs, but the absolute value of the saturation current is not affected by τ and is always equal to

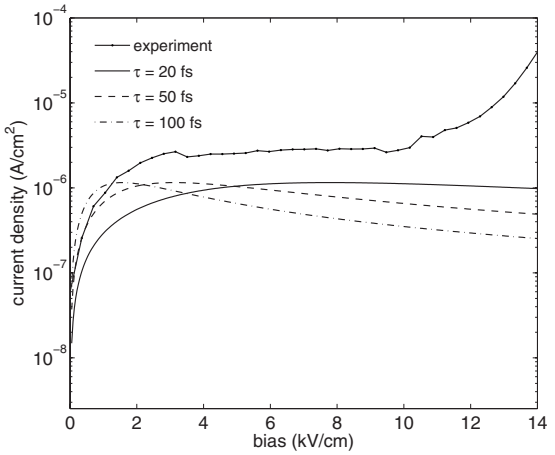

FIG. 3. Low field *IV* curve computed by the high-density Esaki-Tsu mode for $\tau=100$ fs (dash-dot line), $\tau=50$ fs (dashed line) and $\tau=20$ fs (continuous line). Circles show experimental data at 10 K.

$$j_{\mathrm{sat}} = \frac{eN_{3\mathrm{D}}L_z\epsilon^2}{16\hbar E_F} = \frac{1}{4}\frac{e}{\hbar}\rho(\hbar\Omega)^2 \tag{3}$$

where $\rho=m^*/\pi\hbar^2$ is the two-dimensional (2D) density of states and $\hbar\omega$ is the coupling energy between the ground states of two neighboring quantum wells. The rightmost term of the equation allows for a simple and straightforward interpretation of the saturation current: it is due to a fraction of the electrons contained in a narrow energy band close to the Fermi surface oscillating from one well to the other.

The theoretical curve in Fig. 3 is able to follow closely the experimental data up to fields of about 10 kV/cm, where a sudden increase in the current is present: we shall assume that this is the point where the high-field region begins.

Anyway it is remarkable that such a simple model holds up to a regime where the Stark shift is well beyond the ground miniband width, this may be justified by the fact that the big (relatively to miniband width) minigap prevents Zener tunneling effects to occur and thus allows for a simple single miniband transport description.

Even though this model reproduces well the low-field current, there is still a flaw in it. Equation (3) shows that the saturation current contains the ratio between the doping density $N_{3\mathrm{D}}$ and the Fermi energy. Although the Fermi energy is in principle temperature dependent it can be assumed that in a 2D system its value is proportional to the electron density, thus the ratio $N_{3\mathrm{D}}/E_F$ is a constant and the saturation current does not depend on the doping. This assertion is in contrast with what is commonly observed in practice, where the tunneling currents should have at least a linear dependence on the doping.

From a theoretical point of view the reason why this is happening is clear: in the miniband picture a completely filled miniband does not contribute to the current, thus all those electrons that do not have enough in-plane kinetic energy to cross the chemical potential do not affect the total current. This is made clear by the term ϵ/E_F that appears in Eq. (A16), which tells us that the only electrons contributing to the current are those contained in a narrow energy band close to the Fermi surface. When an electron is added to the system it will lie above the others and thus it will lie in such narrow band and will increase the current, but at the same time the chemical potential will be raised pushing another electron out of the bottom of such band.

C. Low temperature and high-bias regime

In the high-bias region coupling between the ground and excited states or the continuum due to the electric field is to be expected. The most natural basis to handle these effects is the one provided by localized Wannier-Stark states in which such processes can be regarded as resonant tunneling effects or field-assisted thermionic emission.

Regarding resonant tunneling contributions a quick calculation shows that the alignment between the ground state of a QW and the excited state of the following one is reached at around 20 kV/cm. Well before this regime the excited state is actually pushed into the continuum and thus a description in terms of resonant tunneling between localized states would not be appropriate. In addition field-assisted thermionic emission should play an increasing role with increasing electric field as the triangular barrier that separates the ground state from the continuum becomes thinner. We shall then describe both effects in terms of electrons tunneling out of the ground state directly in the continuum through thick barrier made up of the neighboring QWs and barriers. With the use of the modified transfer-matrix method[12] one is able to write down an analytical expression of the transmission coefficient $\mathcal{T}$ of such barrier, as explained in detail in Appendix B, and once the latter is known we can compute the ground state to continuum tunnel current as

$$j_{0\to c} = eN_{2\mathrm{D}}\frac{E}{h}\mathcal{T}, \tag{4}$$

where $N_{2\mathrm{D}}$ is the electron sheet density E is the carrier energy above the well bottom.

Depending on the applied field the electrons in the ground state of a QW will have to tunnel through a certain number of neighboring stages before reaching the continuum, and even at that point their motion will be heavily influenced by the superlattice potential, at least until they have enough energy that they can be considered as being moving in an unperturbed linear potential, i.e., their energy above the barrier is much greater than the barrier height itself. Thus the key point is the definition of the effective barrier seen by electrons: in principle one should write the transmission coefficient for all the superlattice periods from a certain well to the contacts, but this is not feasible because of numerical instabilities in the evaluation of Airy functions at high energies, so one has to define an effective barrier length.

Figure 4 shows the transmission coefficient from the ground state of a QW to the continuum computed using a barrier consisting of 1, 2, or 3 superlattice periods. It can be seen that the major difference lies in the low-field behavior: if we consider a barrier made of just one lattice period (barrier+well) we are allowing the electron to tunnel into the continuum even at low fields because the effective barrier width coincides with the AlGaAs barrier between two wells.

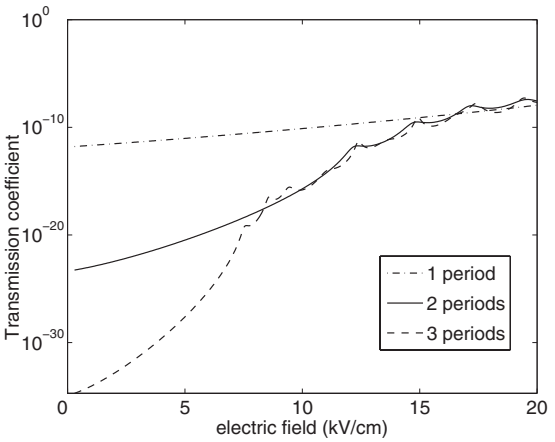

FIG. 4. Transmission coefficient of 1, 2, and 3 superlattice periods as a function of electric field. When the electric field is high enough that the electrons can escape into the continuum through one trapezoidal value the three curves almost coincide but at low fields the presence of an additional barrier strongly reduces the transmission.

By adding another period the low-field transmission is killed and high-field resonances show up due to the coupling of the QWs. The presence of a third period further lowers the low-field transmission and adds more high-field resonances.

Such resonances are not observed in the experimental data and are due to the fact that this model lacks any scattering/dephasing mechanisms that would provide the broadening necessary to smooth the curve. Thus we decided to use a two-period barrier in order to keep artificial resonances at minimum.

D. High-temperature regime

In the high-temperature regime thermal activation of the higher states occurs and thus the j_ν and $j_{\nu\to c}$ with $\nu>0$ become relevant. The miniband currents can be now computed by the standard Esaki-Tsu model since the Fermi level is always well below the lower miniband edge and thus the low-density approximation applies. We can then use Eq. (A5) to compute the average velocity and write the miniband current of νth miniband as

$$j_\nu = N_{3D}\frac{k_B T}{E_F}\exp\left(-\frac{E_\nu - E_F}{k_B T}\right)\frac{\epsilon_\nu}{4}\frac{F\tau}{\frac{\hbar^2}{e^2 L_z^2}+(F\tau)^2}, \qquad (5)$$

where a thermal activation mechanism has been included which accounts for the increase in the νth miniband by the effect of temperature.

The field-assisted tunneling currents $j_{\nu\to c}$ are computed within the same transmission coefficient approximation as for the low-temperature high-field currents with thermal activation added,

$$j_{\nu\to c} = eN_{2D}\frac{k_B T}{E_F}\exp\left(-\frac{E_\nu - E_F - \eta e F L_w}{k_B T}\right)\frac{E}{h}\mathcal{T}_\nu(F). \qquad (6)$$

where $\mathcal{T}_\nu$ is the transmission coefficient of the barrier seen by electrons in state ν. The coefficient η is a geometrical parameter used to obtain the exponential asymptote observed in the high-temperature IV curves at high electric fields. Its physical interpretation is related to the fact that the interlevel spacing and effective barrier lowering effects depend on the applied electric field in a way that is related on the actual shape of the QW, and thus is not easily analytically quantifiable. A precise evaluation of η would in principle be possible by careful computation of the realistic conduction-band profile at different electric fields, employing a self-consistent Schrödinger-Poisson solution and including the effect of Al diffusion into the wells, which is beyond the scope of the current paper.

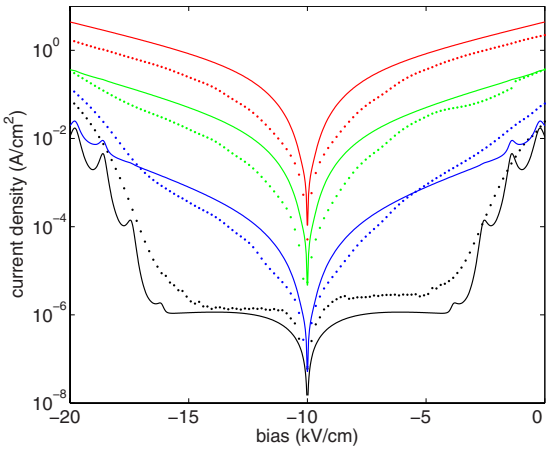

FIG. 5. (Color online) Comparison between computed IV curves (lines) and experimental data (dots) at temperatures of 10 (black), 40 (blue), 50 (green), and 60 K (red).

In addition, setting $\eta=0$ would just change the high-temperature and high-bias region of the IV curves, replacing the exponential asymptote with an horizontal one due to the saturation of the transmission coefficient toward the value $\mathcal{T}=1$. For the device under study it is found that for $\eta=1$ the high-temperature high-field behavior is well reproduced.

IV. RESULTS AND DISCUSSION

The model presented so far has been applied to compute the IV curve of the device described in Sec. II. Figure 5 shows a comparison between the experimental data (dots) and the computed IV curve (lines) at temperatures of 10 (bottom curve), 40, 50 and 60 K (top curve) where the theoretical curves are computed by setting $\tau=20$ fs. The model can be considered to agree quantitatively with the experiment on the whole electric field and temperature range, keeping into account that the discrepancies in the high-temperature currents correspond to a temperature shift of about 5 K.

The low-temperature high-field current resonances in the theoretical curve are an artifact of the fully wavelike nature of the model involved, where the current is proportional to the transmission coefficient of a barrier. A more refined model should also take into account in-plane scattering/dephasing processes that would broaden the peaks and lead to a smoother curve.

Despite the lack of doping dependence the low-field current is well reproduced, and as a further check we have mea-

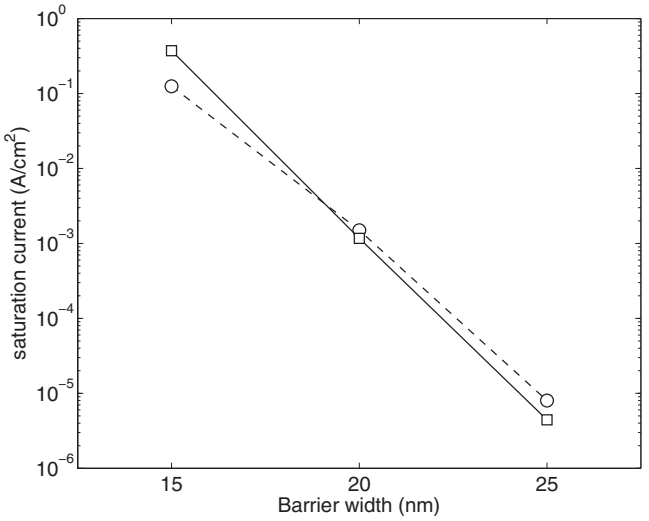

FIG. 6. Computed (squares) and measured (circles) saturation current for three additional devices with 26% Al concentration, 5 nm well and varying barrier width of 15, 20, and 25 nm.

sured the low-temperature saturation current of three additional devices with varying barrier width. These devices have an Al concentration of 26%, well width of 5 nm and barrier width of 15, 20, and 25 nm, respectively. As can be seen in Fig. 6 the computed saturation current agrees quantitatively with the measured one without the use of free parameters, since the plateau current does not depend on τ.

Anyway it must be noted that the plateau current in Eq. (3) has a quadratic dependence on the miniband width, which in turn has an exponential dependence on barrier width and height and thus it is very sensitive to errors in the evaluation of such quantities. In particular, for the device described in Sec. II, which has a nominal miniband width of 30 neV, the combined effect of a 3–6 Å error in barrier width (one to two monolayers) and a ± 5 meV error in the barrier height ($\approx$0.5% Al concentration error) would lead to miniband widths comprised between 56 and 15 neV, leading to a variation in the low-field current of more than 1 order of magnitude.

This barrier height uncertainty effect is also visible in Fig. 6. It can be seen that although the agreement is good, there is a slight slope difference between the experimental data and the computed currents: this could well be due to an error in the evaluation of the miniband height.

Figures 7 and 8 show the relative values of the current contributions that have been considered for the calculation, at 20 and 50 K, respectively. It can be seen that each temperature and electric field regime is dominated by one specific contribution. At 20 K the low-bias current is due to the ground miniband current, j_0 while at high fields is the ground-to-continuum tunneling current $j_{0\to c}$ which dominates. At 50 K both these contributions are negligible when confronted with the excited-state-to-continuum tunneling current $j_{1\to c}$ over the whole bias range. Upper miniband currents j_1 and j_2 never play a significant role in the total current and could thus be neglected.

It is also useful to compare the low-field predictions of the miniband model proposed here with other models based on

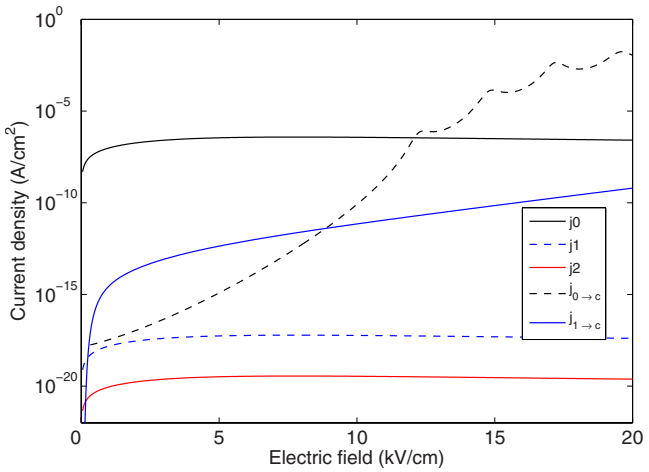

FIG. 7. (Color online) Separated view of all the current components used to compute the IV curves in Fig. 5 at 20 K. The dominant contributions are the ground miniband current at low fields and the groun-to continuum tunneling current at high bias.

localized states. In particular we compare our results with the density-matrix based second-order resonant tunneling theory from Willemberg *et al.*[13] which has been recently applied to the description of tunneling in quantum cascade lasers.[14] In Ref. 13 the Kazarinov-Suris resonant tunneling theory is extended to include second-order terms coming from intrasubband elastic scattering; this leads to the following expression for the current density between two quantum wells:

$$j = \frac{e}{\hbar}(\hbar\Omega)^2 \sum_k \frac{\gamma_k^1(f_k^2 - f_{q_+}^1) + \gamma_k^2(f_{q_-}^2 - f_k^1)}{\Delta^2 + (\gamma_k^1 + \gamma_k^2)^2}, \tag{7}$$

where $\hbar\Omega$ is the coupling energy between wells, f_k^i is the number of electrons in the ith quantum well with planar wave vector k, γ_k^i is the broadening of the same state due to

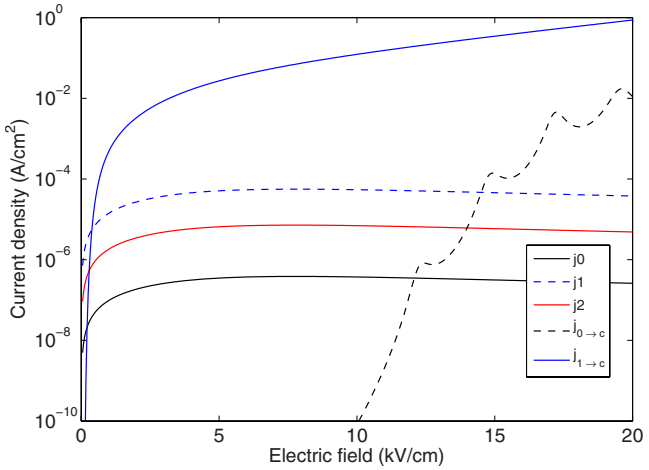

FIG. 8. (Color online) Separated view of all the current components used to compute the *IV* curves in Fig. 5 at 50 K. Current coming from electrons tunneling from the first-excited state into the continuum is clearly dominant over the whole bias range.

elastic scattering, $\Delta = eFL_z$ is the detuning from resonance and $q_{\pm} = \sqrt{k^2 \pm \frac{2m}{\hbar}\Delta}$.

Considering a constant broadening γ and assuming a zero-temperature Fermi distribution of electrons in each well it is possible to rewrite the current as

$$j = \frac{e}{\hbar}(\hbar\Omega)^2 \frac{\rho\Delta\gamma}{\Delta^2 + (2\gamma)^2}. \tag{8}$$

Such result can be easily interpreted as being the tunneling current due to electrons in the initial subband which are able to find free states in the final subband: their number is $\rho\Delta$ and the current is weighted by a Lorentzian whose width is given by γ. Such current has a maximum for $\Delta = 2\gamma$ where it reaches the value $j_{\mathrm{sat}} = \frac{1}{4}\frac{e}{\hbar}\rho(\hbar\Omega)^2$, which is exactly what is given in Eq. (3) considering that $\hbar\Omega = \epsilon/2$.

Anyway as soon as $\rho\Delta$ becomes equal to the Fermi energy Eq. (8) is no more valid because it would imply that the number of electrons tunneling between wells is greater than electron sheet density $N_{2\mathrm{D}} = \rho E_F$. Thus for $\Delta > E_F$ we have to clamp Δ at E_F and rewrite Eq. (8) as

$$\begin{cases} j = \dfrac{e}{\hbar}(\hbar\Omega)^2 \dfrac{\rho\Delta\gamma}{\Delta^2 + (2\gamma)^2} & \text{for } \Delta \le E_F \\ j = \dfrac{e}{\hbar}(\hbar\Omega)^2 N_{2\mathrm{D}} \dfrac{\gamma}{\Delta^2 + (2\gamma)^2} & \text{for } \Delta > E_F. \end{cases} \tag{9}$$

This way after an initial linear current increase, a saturation regime is predicted where the number of tunneling electrons is no more increased by the electric field because the initial subband bottom is above the maximum energy of electrons in the final one, giving the maximum possible tunneling rate. On the other hand, as the field increases the system is more off-resonant and thus the current decreases as a γ-broadened Lorentzian, in qualitative disagreement with observations. However, a constant field drop across the superlattice has been assumed in the negative differential conductance region; whereas experiments have shown that this is not the case and electric field domain formation has to be expected[15] and this would lower the actual detuning between subbands. Eventually, this effect could lead to the clamping of the current to its $\Delta = E_F$ value, giving rise to the plateau behavior with a saturation current given by

$$j_{\mathrm{sat}} = \frac{e}{\hbar}(\hbar\Omega)^2 N_{2\mathrm{D}} \frac{\gamma}{E_F^2 + (2\gamma)^2}, \tag{10}$$

which, in the case $2\gamma > E_F$ reduces to

$$j_{\mathrm{sat}} = \frac{1}{4}\frac{e}{\hbar} N_{2\mathrm{D}} \frac{(\hbar\Omega)^2}{\gamma}. \tag{11}$$

The latter equation is again very similar to Eq. (3) the only difference being that the Fermi energy at the denominator has been replaced here by the in-plane broadening energy. This gives the saturation current a linear dependence on doping, a feature which is missing in the miniband model and that is to be expected in a real system, and at the same time justifies why the miniband model is found to work in a condition where the miniband width is much lower than the Stark shift. The reason is that typical values of the in-plane broadening energy are of the same order than the Fermi energy of electrons in QWIP systems, thus making Eqs. (3) and (11) numerically equivalent. Anyway it must be noted that Eq. (11) has been obtained by dropping the homogeneous field approximation and speculating that the value of the saturation current is clamped at the value it reaches for $\Delta = E_F$. Thus a quantitative evaluation of the actual field distribution should be performed before using Eq. (11) to evaluate the plateau current, which is beyond the scope of the present paper. Nevertheless from the above reasoning we can get further insight into the physical interpretation of the miniband model and say it can be thought as a low-order approximation of a more general theory which should include second-order tunneling as well as field inhomogeneity effects which is working when the Fermi and in-plane broadening energies are comparable.

V. SUMMARY AND CONCLUSIONS

We developed a model for the evaluation of dark current in mid-IR QWIPs over a wide electric field and temperature range. We have addressed the low-field and the high-field regions of the dark *IV* curve using two different approaches: the miniband and Wannier-Stark pictures, respectively. The low-field miniband model is based on the high-density correction of the Esaki-Tsu model, in order to correctly handle the case where the Fermi energy lies above the upper edge of the ground miniband. Due the extremely low coupling between wells the miniband widths are of the order of tens of neV due to the exponential dependence on the barrier width and height. Even though with this extremely narrow minibands one is usually led to drop the miniband picture in favor of the localized Wannier-Stark basis, by using this model we are able to derive an analytical expression for the low-field dark current at low temperatures which quantitavely agrees with the measured data from four different devices without using any fitting parameter.

Up to 30 K the miniband based model is found to reproduce the experimental data up to 10 kV/cm; after this threshold the high-field region begins and the experiment shows a consistent deviation from the theoretical curve. We then switch to a Wannier-Stark picture in which the current is dominated by field-assisted tunneling from the ground state of the QWs directly into the continuum. By using a modified transfer-matrix formalism we derived an analytical expression for the transmission coefficient of trapezoidal barriers, which allowed us to compute the tunneling rates. Again we find quantitative agreement with experimental data with no fitting parameters.

One fundamental limitation of the proposed model is that the computed low-field current density lacks dependence on the doping density, a feature which is intrinsic in the miniband description. Anyway since the doping levels in QWIPs are such that the distance between the Fermi level and the ground state is always approximately the same, this is not a major issue as also confirmed by the fact that the low-field current is correctly reproduced for four different devices. We justify the lack of doping dependence in the model by comparing it to a higher order model and introducing electric

field inhomogeneities. This comparison suggests that the lack of doping dependence is due to the fact that the miniband model is a low-order approximation of a more general theory. In addition, any quantitative agreement must be interpreted in view of the fact that in these structures the tunneling current are very sensitive to the barrier height and width. We show that within the proposed model a small error of ± 5 meV in the barrier height and ± 0.5 nm in barrier width can determine current fluctuations of more than 1 order of magnitude.

In the high-temperature region field-assisted thermionic emission is found to dominate regardless of the applied electric field, as already pointed out by previous models.

APPENDIX A: LOW-FIELD CURRENT DENSITY

We shall start considering the three-dimensional miniband structure of the device. Due to the extremely strong confinement of electrons in the quantum wells the miniband dispersion is sinusoidal with very good approximation, while we shall consider parabolic bands in the continuum. Thus we can write the complete band structure as

$$E_\nu(\mathbf{k}) = E_\nu + \frac{\epsilon_\nu}{2}(1-(-1)^\nu \cos(k_z L)) + \frac{\hbar^2 k_\parallel^2}{2m} \tag{A1}$$

where E_ν is the lowest energy of νth miniband, ϵ_ν is the miniband width, k_z and $k_\parallel$ are the growth-direction and in-plane parts of the electron wave vector and L_z is the superlattice periodicity.

From now on we shall drop the index ν and refer to the ground miniband only ($\nu=0$) since it is the only populated one at low temperature. From the analytic expression of the band structure we can write the group velocity $\mathbf{v}=\nabla E/\hbar$ as

$$\mathbf{v}_\nu(\mathbf{k}) = \frac{\epsilon L}{2\hbar}\sin(k_z L)\hat{\mathbf{u}}_z + \frac{\hbar k_\parallel}{m}\hat{\mathbf{u}}_\parallel. \tag{A2}$$

At thermal equilibrium the distribution function is given by

$$f(\mathbf{k}) = f(k_z,k_\parallel) = \frac{1}{1+e^{E(k_z,k_\parallel)-\mu/k_B T}}, \tag{A3}$$

where μ is the electron chemical potential. Once f is known we can use it to compute the average current density $\mathbf{j}$ as

$$\mathbf{j} = eN_{3D}\frac{\int \mathbf{v}_\nu(\mathbf{k}) f(\mathbf{k}) \mathrm{d}\mathbf{k}}{\int f(\mathbf{k})\mathrm{d}\mathbf{k}}. \tag{A4}$$

It is easy to see that at thermal the integral evaluates to 0 since f is symmetric in k space.

In the miniband picture the effect of bias is to translate the distribution function in the direction of the applied field. In absence of scattering this gives rise to the well-known Bloch oscillations, but if we assume a certain momentum relaxation time τ then we can compute the average speed reached by an electron initially at $k_z=0$ by means of the Esaki-Tsu model as

$$v_{ET} = \frac{\epsilon L}{2\hbar}\frac{\xi}{1+\xi^2}, \tag{A5}$$

where $\xi = eF\tau L/\hbar$. Within the sinusoidal miniband approximation the corresponding drift in k space can be computed as

$$\Delta k_z(F) = \frac{1}{L}\arcsin\left(\frac{2\hbar}{\epsilon L}v_{ET}\right). \tag{A6}$$

where the dependence on the electric field is hidden in v_{ET}.

In the case of high electron density we shall assume that the whole distribution function is drifted by this amount, breaking its symmetry and giving rise to a current. The *IV* curve can then be obtained as

$$\mathbf{j}(F) = eN_{3D}\frac{\int \mathbf{v}(\mathbf{k}) f(\mathbf{k}+\Delta k_z(F)\hat{\mathbf{u}}_z)\mathrm{d}\mathbf{k}}{\int f(\mathbf{k})\mathrm{d}\mathbf{k}}. \tag{A7}$$

In order to find an analytical solution we can perform some approximations exploiting the fact that the minibands are extremely narrow and the temperature is low. As long as $k_B T < \mu$ we can compute the integral at the denominator in Eq. (A7) as the volume V_k of a cylinder in k space, whose radius corresponds the Fermi in-plane wave vector $k_\parallel^F = \sqrt{2m\mu/\hbar^2}$ and whose height is $2\pi/L$ obtaining

$$V_k = \frac{4\pi^2 m\mu}{\hbar^2 L}. \tag{A8}$$

In the limit $\epsilon \ll k_B T$ the Fermi-Dirac distribution is a slowly varying function over the miniband and thus we can linearize it as

$$f(k_z,k_\parallel) = f(0,k_\parallel) + \left.\frac{\mathrm{d}f}{\mathrm{d}E}\right|_{k_z=0}[E(k_z,k_\parallel) - E(0,k_\parallel)], \tag{A9}$$

which results in

$$f(k_z,k_\parallel) = f(0,k_\parallel) + \frac{\epsilon}{2}\frac{\partial f}{\partial k_\parallel}\left.\frac{\partial k_\parallel}{\partial E}\right|_{k_z=0}[1-\cos(k_z L)]. \tag{A10}$$

Combining this latter equation with the immediately verifiable relation,

$$\left.\frac{\partial k_\parallel}{\partial E}\right|_{k_z=0} = \frac{m}{\hbar^2 k_\parallel}, \tag{A11}$$

we get

$$f(k_z,k_\parallel) = f(0,k_\parallel) + \frac{\epsilon m}{2\hbar^2 k_\parallel}[1-\cos(k_z L)]\left.\frac{\partial f}{\partial k_\parallel}\right|_{k_z=0}. \tag{A12}$$

Within this approximation we can now explicitly compute the integral in Eq. (A7) in cylindrical coordinates as

$$\mathbf{j}(F) = \frac{eN_{3D}}{V_k}\int_0^{2\pi}\int_0^{\infty}\int_{-\pi/L}^{\pi/L}\left[\frac{\epsilon L}{2\hbar}\sin(k_z L)\hat{\mathbf{u}}_z + \frac{\hbar k_\parallel}{m}\hat{\mathbf{u}}_\parallel\right]\left\{f(0,k_\parallel) + \frac{\epsilon m}{2\hbar^2 k_\parallel}[1-\cos(k_z L+\Delta k_z)]\left.\frac{\partial f}{\partial k_\parallel}\right|_{k_z=0}\right\}k_\parallel dk_z dk_\parallel d\theta. \tag{A13}$$

From symmetry considerations it can be deduced that the only nonzero term in the integral is the z component of the current given by

$$j_z(F) = -\frac{eN_{3D}\epsilon^2 Lm}{4\hbar^3 V_k}\int_0^{2\pi}\int_0^{\infty}\int_{-\pi/L}^{\pi/L}\sin(k_z L)\cos(k_z L+\Delta k_z)\times\left|\frac{\partial f}{\partial k_\parallel}\right|_{k_z=0} dk_z dk_\parallel d\theta. \tag{A14}$$

Performing the integrations along θ and $k_\parallel$ and using the sum rule for the cosine function we get

$$j_z(F) = \sin(\Delta k_z L)\frac{\pi^2 eN_{3D}\epsilon^2 m}{2\hbar^3 V_k}f(E_0), \tag{A15}$$

where $f(E_0)$ denotes the value of the Fermi-Dirac distribution function at the lowest edge of the miniband. Substituting in the last equation the expressions of V_k and Δk_z from Eqs. (A8) and (A6) we get

$$j_z(F) = eN_{3D}v_{ET}\frac{\epsilon}{4\mu}f(E_0). \tag{A16}$$

From this we see that the current obtained by the Esaki-Tsu model has to be corrected by the ratio between the miniband width and the chemical potential. This is exactly the result obtained by Lebwohl and Tsu in Ref. 11 for the case in which the Fermi energy is above the upper miniband edge at $T=0$. Finally, considering Eq. (A5) we can write the final form of the IV curve as

$$j_z(F) = N_{3D}\frac{F\tau}{\frac{\hbar^2}{e^2L^2}+(F\tau)^2}\frac{\epsilon^2}{8\mu}f(E_0). \tag{A17}$$

APPENDIX B: TRANSMISSION COEFFICIENTS FROM MODIFIED TRANSFER MATRIX METHOD

The method introduced by Rakityansky[12] allows to devise an approximation less closed-form expression for the transfer matrix of any quantum device which can be separated into sections for which a closed solution of the Schrödinger equation exists. Here we will apply the concept to piecewise linear potential profiles.

A modified transfer matrix has the form,

$$\mathcal{M}(x) = \begin{pmatrix}\phi(x) & \chi(x)\\ \phi'(x) & \chi'(x)\end{pmatrix}, \tag{B1}$$

where $\phi(x)$ and $\chi(x)$ are two linearly independent solutions of the one-dimensional (1D) stationary Schrödinger equation for a potential profile $V(x)$ which satisfy the conditions,

$$\phi(0)=1 \quad \chi(0)=0, \tag{B2}$$

$$\phi'(0)=0 \quad \chi'(0)=1, \tag{B3}$$

so that one can express the wave function $\psi(x)$ and its derivative $\psi'(x)$ as a function of $\psi(0)$ and $\psi'(0)$ as

$$\begin{pmatrix}\psi(x)\\ \psi'(x)\end{pmatrix} = \mathcal{M}(x)\begin{pmatrix}\psi(0)\\ \psi'(0)\end{pmatrix}. \tag{B4}$$

With this definition of the transfer matrix one can compute the transmission coefficient of a device enclosed between two constant potentials in the form,

$$\mathcal{T} = \left|\frac{2\sqrt{k_1 k_2}}{k_1\mathcal{M}_{22}+k_2\mathcal{M}_{11}-ik_1k_2\mathcal{M}_{12}+i\mathcal{M}_{21}}\right|^2 \tag{B5}$$

where k_1 and k_2 are the electron wave vectors on the left and right side of the device.

The transfer-matrix elements of for a trapezoidal barrier of width L, height E_0 with equivalent electric field F are

$$\mathcal{M}_{11} = \pi[\mathrm{Bi}'(\theta_0)\mathrm{Ai}(\theta) - \mathrm{Ai}'(\theta_0)\mathrm{Bi}(\theta)], \tag{B6}$$

$$\mathcal{M}_{12} = \frac{\pi}{\kappa}[-\mathrm{Bi}(\theta_0)\mathrm{Ai}(\theta) + \mathrm{Ai}(\theta_0)\mathrm{Bi}(\theta)], \tag{B7}$$

$$\mathcal{M}_{21} = \pi\kappa[\mathrm{Bi}'(\theta_0)\mathrm{Ai}'(\theta) - \mathrm{Ai}'(\theta_0)\mathrm{Bi}'(\theta)], \tag{B8}$$

$$\mathcal{M}_{22} = \pi[-\mathrm{Bi}(\theta_0)\mathrm{Ai}'(\theta) + \mathrm{Ai}(\theta_0)\mathrm{Bi}'(\theta)], \tag{B9}$$

with

$$\kappa = \mathcal{F}^{1/3}, \tag{B10}$$

$$\theta_0 = -\frac{\mathcal{E}-\mathcal{E}_0}{\kappa^2}, \tag{B11}$$

$$\theta = \kappa L + \theta_0, \tag{B12}$$

where

$$\mathcal{F} = e\frac{2m}{\hbar^2}F, \tag{B13}$$

$$\mathcal{E} = \frac{2m}{\hbar^2}E, \tag{B14}$$

$$\mathcal{E}_0 = \frac{2m}{\hbar^2}E_0, \tag{B15}$$

where E is the electron energy.

[1] B. F. Levine, J. Appl. Phys. **74**, R1 (1993).
[2] S. Panda, B. K. Panda, and S. G. Mishra, Phys. Rev. B **69**, 195304 (2004).
[3] T. Osotchan, V. W. L. Chin, and T. L. Tansley, Phys. Rev. B **54**, 2059 (1996).
[4] C. Koeniguer, G. Dubois, A. Gomez, and V. Berger, Phys. Rev. B **74**, 235325 (2006).
[5] A. Gomez, N. Pere-Laperne, L. A. de Vaulchier, C. Koeniguer, A. Vasanelli, A. Nedelcu, X. Marcadet, Y. Guldner, and V. Berger, Phys. Rev. B **77**, 085307 (2008).
[6] W. Ryzhii, M. Rjzii, and H. C. Liu, J. Appl. Phys. **92**, 207 (2002).
[7] H. Willenberg, O. Wolst, R. Elpelt, W. Geisselbrecht, S. Malzer, and G. H. Dohler, Phys. Rev. B **65**, 035328 (2002).
[8] E. Ciancio, R. C. Iotti, and F. Rossi, Phys. Rev. B **69**, 165319 (2004).
[9] F. Castellano, R. C. Iotti, and F. Rossi, J. Appl. Phys. **104**, 123104 (2008).
[10] L. Esaki and R. Tsu, IBM J. Res. Dev. **14**, 61 (1970).
[11] P. A. Lebwohl and R. Tsu, J. Appl. Phys. **41**, 2664 (1970).
[12] S. A. Rakityansky, Phys. Rev. B **70**, 205323 (2004).
[13] H. Willenberg, G. H. Dohler, and J. Faist, Phys. Rev. B **67**, 085315 (2003).
[14] R. Terazzi, T. Gresch, A. Wittmann, and J. Faist, Phys. Rev. B **78**, 155328 (2008).
[15] K. K. Choi, B. F. Levine, R. J. Malik, J. Walker, and C. G. Bethea, Phys. Rev. B **35**, 4172 (1987).